Am J Cancer Res 2026;16(10):4462-4480
www.ajcr.us /ISSN:2156-6976/ajcr0174891

Original Article

Radiogenomic associations of PIK3CA and TP53 alterations with multidimensional ultrasonographic phenotypes of breast cancer

Huiming Li, Tao Cheng

Department of Ultrasound, Changzhou Fourth People's Hospital, Changzhou 213000, Jiangsu, China

Received June 22, 2026; Accepted September 2, 2026; Epub October 15, 2026; Published October 30, 2026

Abstract: This study aimed to investigate the intrinsic links between abnormalities in the core driver genes PIK3CA and TP53 and multidimensional ultrasonographic features of breast cancer, thereby providing imaging-based evidence for the noninvasive assessment of driver gene status. Using data from The Cancer Genome Atlas (TCGA), we first performed bioinformatic analyses of the pan-cancer expression patterns, prognostic significance, and immune infiltration relevance of PIK3CA and TP53. We then performed a single-center retrospective cross-sectional analysis of 201 patients with primary breast cancer treated at our hospital between January 2023 and October 2025; postoperative follow-up was unavailable for this hospital cohort. Bioinformatic analyses showed that PIK3CA and TP53 were highly expressed in breast cancer, and that elevated expression of either gene was associated with poorer overall survival, but showed no correlation with tumor immune cell infiltration. In the clinical cohort, the overall mutation rates of PIK3CA and TP53 were 35.8% and 28.4%, respectively, and the mutation statuses of the two genes were significantly associated (P=0.006). The mRNA expression levels of both genes were higher in breast cancer tissues than in matched adjacent normal tissues, and were also higher in mutant tumors than in wild-type tumors (P<0.05). Taken together, these findings suggest that PIK3CA and TP53 alterations are associated with distinct ultrasonographic phenotypes of breast cancer, providing preliminary imaging clues for understanding radiogenomic heterogeneity rather than a validated noninvasive test for driver-gene status.

Keywords: Breast cancer, PIK3CA, TP53, ultrasonography, radiogenomics, driver gene

Introduction

Breast cancer is the most common malignant tumor in women worldwide and remains the leading cause of cancer-related death among women [1]. According to the GLOBOCAN 2022 estimates, approximately 2.3 million women were diagnosed with breast cancer worldwide in 2022, and about 670,000 deaths were attributed to the disease, indicating that breast cancer remains a major global health burden [2]. BC is marked by pronounced genomic heterogeneity, and somatic alterations in driver genes together with dysregulated transcriptional expression are now regarded as central events in tumor initiation, malignant progression, and therapeutic resistance [3]. In studies on the molecular pathogenesis of cancer, PIK3CA and TP53 have consistently been identified as the two core driver genes with the highest mutation frequencies in BC, with overall mutation rates of 30%-40% and 20%-35%, respectively [4, 5]. Functional abnormalities in these genes not only directly influence tumor cell proliferation, invasion, and metastatic potential, but also bear closely on treatment selection and clinical outcome, making them key biomarkers in the precision management of BC [6].

At present, however, definitive identification of driver-gene abnormalities still depends largely on tissue-based molecular testing. The invasive nature of tissue-based testing, together with intratumoral sampling heterogeneity and limited feasibility for repeated dynamic monitoring, limits its broader application in clinical screening and whole-course tumor management [7]. Ultrasound is the preferred noninvasive imaging modality for BC evaluation. It is radiation-

https://doi.org/10.62347/ILHE4769

free, convenient, accessible, and readily repeatable, and has become a core tool for early screening, lesion localization, and preoperative assessment [8]. Previous studies have shown that ultrasonographic features of BC are closely related to molecular subtype and malignant biological behavior, and some morphologic phenotypes may indirectly reflect the underlying genomic profile of the tumor, raising the possibility that tumor gene status could be assessed in a noninvasive manner [9, 10].

However, most published studies have focused on isolated associations and have not systematically examined phenotypic heterogeneity across hotspot mutations, limiting clinical translation [11-13]. In the present study, we analyzed the correlations of PIK3CA and TP53 with conventional grayscale morphology and color Doppler blood-flow features of BC in order to define sonographic phenotypes associated with gene abnormalities. The results may provide preliminary imaging evidence for understanding the radiogenomic associations between driver-gene alterations and ultrasound phenotypes in BC, thereby offering a basis for future model-based studies and prospective validation.

Materials and methods

Bioinformatics analysis

Public databases were used to analyze the expression characteristics, prognostic value, and immune infiltration relevance of PIK3CA and TP53, thereby providing a theoretical basis for subsequent validation in clinical samples. All analytical data were obtained from The Cancer Genome Atlas (TCGA), including transcriptomic sequencing data from 33 malignant tumor types across the pan-cancer spectrum. Based on the TCGA dataset, we first performed a pan-cancer expression profile analysis of PIK3CA and TP53, comparing their expression levels between tumor tissues and matched normal tissues across different cancer types. Patients were then divided into high- and low-expression groups according to the median expression level of each gene. Kaplan-Meier survival curves for overall survival were plotted to evaluate the relationship between gene expression and patient prognosis. In addition, immune infiltration analysis was performed using the TIMER2.0 online platform based on TCGA-BRCA RNA-sequencing data. SangerBox was used only as an online bioinformatics analysis and visualization platform for public TCGA-derived data and was not related to Sanger sequencing of the hospital-based cohort. The correlations between PIK3CA or TP53 expression and the estimated abundance of six major immune cell populations, including B cells, CD4+ T cells, CD8+ T cells, macrophages, neutrophils, and dendritic cells, were evaluated using Spearman correlation analysis with adjustment for tumor purity.

Clinical study design

The hospital-based analysis did not include postoperative follow-up; therefore, disease-free survival, overall survival, locoregional recurrence, and distant metastasis were not evaluated in this cohort. The study protocol was approved by the ethics committee of Changzhou Fourth People's Hospital. All analyses were based on anonymized data and residual pathological specimens retained from routine clinical care. The study did not alter the original diagnostic or therapeutic pathway and imposed no additional medical burden or risk on the patients.

Study population

Patients with primary BC who underwent radical mastectomy or breast-conserving surgery in the Department of Breast Surgery of Changzhou Fourth People's Hospital between January 2023 and October 2025 were eligible for inclusion. Initial screening through the hospital medical record system identified 348 cases within the specified period. After stepwise screening according to the predefined inclusion and exclusion criteria, 201 eligible patients were finally included. This study has used clinical residual samples for retrospective study, which has been approved by the Ethics committee of Changzhou Fourth People's Hospital (No.AF/SS-20/05.1), and the informed consent of the patients was waived.

Inclusion criteria

① Postoperative paraffin specimens were reviewed independently and in a blinded manner by two senior pathologists, confirming primary invasive ductal carcinoma or invasive lobular carcinoma of the breast, while excluding spe-

cial histological subtypes such as mucinous carcinoma and medullary carcinoma; ② a standardized breast ultrasound examination had been completed in our ultrasound department within 14 d prior to surgery, including complete two-dimensional grayscale and color Doppler flow imaging data, with original DICOM images fully preserved in the PACS system and of sufficient quality for standardized image review and parameter measurement; ③ paired BC lesion tissue and adjacent normal breast tissue had been collected within 30 min after surgical excision, rapidly frozen in liquid nitrogen, and continuously stored at -80°C before RNA extraction for qRT-PCR analysis, with no prior freeze-thaw cycles and satisfactory RNA quality; archived molecular testing records were available for PIK3CA and TP53 mutation status and reported mutation-site category; ④ complete electronic medical records, pathology reports, imaging reports, and laboratory data were available, with no missing key data for the core variables of this study.

Exclusion criteria

① Any preoperative antitumor treatment, including neoadjuvant chemotherapy, neoadjuvant endocrine therapy, radiotherapy, targeted therapy, or immunotherapy, that might interfere with tumor genetic characteristics or ultrasound manifestations; ② bilateral BC, recurrent BC, metastatic BC, or a previous history of other systemic malignancies; ③ concomitant breast diseases such as acute mastitis, breast abscess, or benign breast tumors that could affect accurate interpretation of ultrasound findings; ④ ultrasound images with motion artifacts, inappropriate gain settings, nonstandard scanning planes, or other problems that precluded standardized parameter measurement; ⑤ severe degradation of tissue specimens or inadequate RNA quality for qRT-PCR analysis, unavailable archived molecular testing records, or incomplete PIK3CA/TP53 mutation status; ⑥ missing core clinicopathological or imaging data that would preclude statistical analysis.

Collection of clinicopathological data

All data were obtained from the archived structured electronic medical record system and the pathology database of our hospital. Two uniformly trained researchers independently extracted the data in a blinded manner and established a standardized Excel database. After data extraction, a third senior researcher performed a complete cross-check. Any discrepancies were resolved through discussion among the three investigators, so that data accuracy and completeness could be ensured as much as possible.

Breast ultrasound examination

All ultrasound images were original data retained from routine preoperative examinations. Imaging was performed using a GE Logiq E9 color Doppler ultrasound system equipped with a high-frequency linear-array transducer, and the operating frequency for breast lesion assessment was mainly maintained within 9-15 MHz according to lesion depth and image quality. Patients were examined in the supine position with both arms raised above the head to fully expose the bilateral breasts and axillary regions. Centered on the nipple, radial scanning combined with transverse and longitudinal sweeps was used to achieve a continuous and systematic examination of both breasts without omission. Once a lesion was identified, two-dimensional grayscale and color Doppler flow imaging were performed on the maximal lesion section and the orthogonal section. Lesion size and morphological features were assessed on the maximal section.

Image review and parameter measurement

Image review and parameter measurement were performed by two physicians with the rank of associate chief physician or above, each with more than 10 years of experience in breast ultrasound diagnosis. A double-blind approach was used throughout image interpretation. Neither physician was aware of the patients' pathological grade, molecular subtype, gene testing results, or the other physician's conclusions. Any disputed images or parameters were resolved by consensus after joint review. To assess reproducibility, 41 examinations, representing 20.4% of the study cohort, were selected using computer-generated random sampling. Both radiologists independently reviewed these examinations while remaining blinded to the clinicopathological and molecular findings and to each other's assessments. Reader 1 repeated the assessment after an interval of at least 2 weeks with-

out access to the initial ratings. Interobserver agreement was evaluated by comparing the first assessments of Readers 1 and 2, whereas intraobserver agreement was evaluated by comparing the two assessments of Reader 1. Linear weighted Cohen's kappa was used for the three-level lesion-size category, and unweighted Cohen's kappa was used for the remaining binary ultrasonographic features. Feature-specific coefficients with 95% confidence intervals are reported in Supplementary Table 2.

Collection and preservation of tissue specimens

All tissue specimens were residual samples after routine pathological examination of surgically resected tissues. Specimen collection was completed jointly by the operating surgeon and the pathologist within 30 min after excision. BC tissue was sampled from the main body of the tumor while avoiding areas of necrosis, hemorrhage, and calcification. Matched adjacent normal breast tissue was collected from glandular tissue located at least 3 cm away from the tumor margin, and postoperative pathology confirmed the absence of tumor cell infiltration. Each specimen weighed at least 50 mg. Before RNA extraction for qRT-PCR analysis, specimen handling logs and RNA quality-control results were reviewed. Samples with any documented thawing event, repeated freeze-thaw exposure, or evidence of RNA degradation were excluded from the expression analysis.

Ascertainment of PIK3CA and TP53 mutation results

PIK3CA and TP53 mutation results were retrospectively extracted from archived institutional molecular reports generated by targeted Sanger sequencing of predefined hotspot regions. According to the laboratory reporting protocol, variants with a mutant allele frequency (MAF) of ≥20% were classified as positive. In this study, "wild type" indicates that no reportable variant was detected within the tested regions above the reporting threshold; it does not exclude low-frequency variants or alterations outside the targeted regions.

Quantitative real-time polymerase chain reaction (qRT-PCR)

Total RNA extraction: Total RNA was extracted from BC tissues and matched adjacent normal tissues using TRIzol reagent (Invitrogen, catalog no. 15596026, USA). Briefly, 50 mg of frozen tissue was ground into powder in liquid nitrogen. Lysis, phase separation, precipitation, and washing were then carried out according to the manufacturer's instructions, and the final RNA pellet was dissolved in RNase-free water.

cDNA reverse transcription: Reverse transcription was performed using the PrimeScript RT Reagent Kit with gDNA Eraser (TaKaRa, catalog no. RR047A, Dalian, China), which simultaneously removes genomic DNA contamination. The gDNA removal reaction contained 2 μL 5×g DNA Eraser Buffer, 1 μL gDNA Eraser, 1 μg total RNA, and RNase-free water added to a final volume of 10 μL, followed by incubation at 42°C for 2 min and then holding at 4°C. Reverse transcription was subsequently carried out by adding 4 μL 5×PrimeScript Buffer, 1 μL PrimeScript RT Enzyme Mix I, 1 μL RT Primer Mix, and RNase-free water to a final volume of 20 μL. The reaction conditions were 37°C for 15 min, 85°C for 5 s, and then 4°C. The resulting cDNA was stored at -20°C, and all subsequent analyses were completed within 1 week.

Real-time quantitative PCR: qRT-PCR was performed on an ABI 7500 Real-Time PCR System using the SYBR Premix Ex Taq II Kit (TaKaRa, catalog no. RR820A, Dalian, China). GAPDH served as the internal reference gene, and the relative mRNA expression levels of PIK3CA and TP53 were measured. Primer specificity was verified using NCBI Primer-BLAST, and the sequences are shown in **Table 1**. The qRT-PCR reaction volume was 20 μL, including 10 μL SYBR Premix Ex Taq II, 0.8 μL each of forward and reverse primers (10 μmol/L), 2 μL cDNA template, and RNase-free water added to 20 μL. The amplification conditions were 95°C for 30 s for initial denaturation, followed by 40 cycles of 95°C for 5 s and 60°C for 34 s. A melting curve analysis was performed after amplification to confirm product specificity, and only samples showing a single melting peak were included in the statistical analysis.

Table 1. Primer sequences used for qRT-PCR detection of PIK3CA and TP53 mRNA expression

	F	R
PIK3CA	5'-GAAGATGCTGGCAAAGATGGA-3'	5'-TCCAGTTTCTTCAGCAGCTTC-3'
TP53	5'-CAGCACATGACGGAGGTTGT-3'	5'-TCATCCAAATACTCCACACGC-3'
GAPDH	5'-GGAGCGAGATCCCTCCAAAAT-3'	5'-GGCTGTTGTCATACTTCTCATGG-3'

Each sample was tested in triplicate. A no-template blank control and a no-reverse-transcription negative control were included at the same time to exclude contamination. Relative mRNA expression levels of PIK3CA and TP53 were calculated using the $2^{-\Delta\Delta Ct}$ method, with matched adjacent normal tissue serving as the calibrator.

Observation indicators

Primary outcomes: ① Archived PIK3CA and TP53 mutation profiles in BC tissues, including overall mutation frequency, reported mutation-site category, and the proportion of each reported site among all mutation-positive cases. Operational definitions: PIK3CA and TP53 mutation status and reported mutation-site categories were extracted from archived molecular testing records. Cases with a reportable alteration within the targeted regions were classified as mutant type, whereas cases without a reportable alteration above the assay threshold were operationally classified as wild type. Reported hotspot categories included E542K, E545K, and H1047R for PIK3CA, and R175H, G245S, and R273H for TP53; other reported sites were classified as rare mutation-site categories. ② Correlation between PIK3CA mutation status and multidimensional ultrasound features of BC: the distributions of conventional grayscale ultrasound features and color Doppler flow imaging findings were compared between patients with wild-type and mutant PIK3CA according to archived mutation records. ③ Correlation between TP53 mutation status and multidimensional ultrasound features of BC: the distributions of the same multidimensional ultrasound features were compared between patients with wild-type and mutant TP53 according to archived mutation records.

Secondary outcomes: ① Coexistence and mutual exclusivity of archived PIK3CA and TP53 mutation status in BC tissues, with analysis of the association between the mutation categories of the two genes. ② Differences in the relative mRNA expression levels of PIK3CA and TP53 between BC tissues and matched adjacent normal breast tissues. ③ Differences in PIK3CA and TP53 mRNA expression in BC tissues according to archived mutation status, including differences between wild-type and mutant tumors and among reported mutation-site categories. ④ Associations between continuous tumor PIK3CA or TP53 mRNA expression and the exploratory composite ultrasonographic phenotype score.

Statistical analysis

All statistical analyses were performed using SPSS 26.0 software (IBM, USA). All tests were two-sided, with $\alpha=0.05$ as the significance level, and $P<0.05$ was considered statistically significant. Continuous variables were first tested for normality using the Shapiro-Wilk test. Data with a normal distribution are presented as mean ± standard deviation, whereas non-normally distributed data are expressed as median and interquartile range [M (P25, P75)]. Categorical variables are presented as counts and constituent ratios (n/%), group comparisons were performed according to data type and study design. For paired continuous data, the paired t test was used when the data were normally distributed; otherwise, the Wilcoxon signed-rank test was applied. For comparisons between two independent groups, the independent-samples t test was used for normally distributed data with homogeneity of variance; otherwise, the Mann-Whitney U test was used. For multiple-group analyses, an omnibus test was performed first. For non-normally distributed mutation-site expression data, the Kruskal-Wallis test was followed, when appropriate, by pairwise Mann-Whitney U tests with Holm adjustment. No unadjusted pairwise inferential comparisons were performed among the four combined mutation-pattern groups. Differences in categorical variables were analyzed using the Pearson χ^2 test, and Fisher's exact test was used when the expected fre-

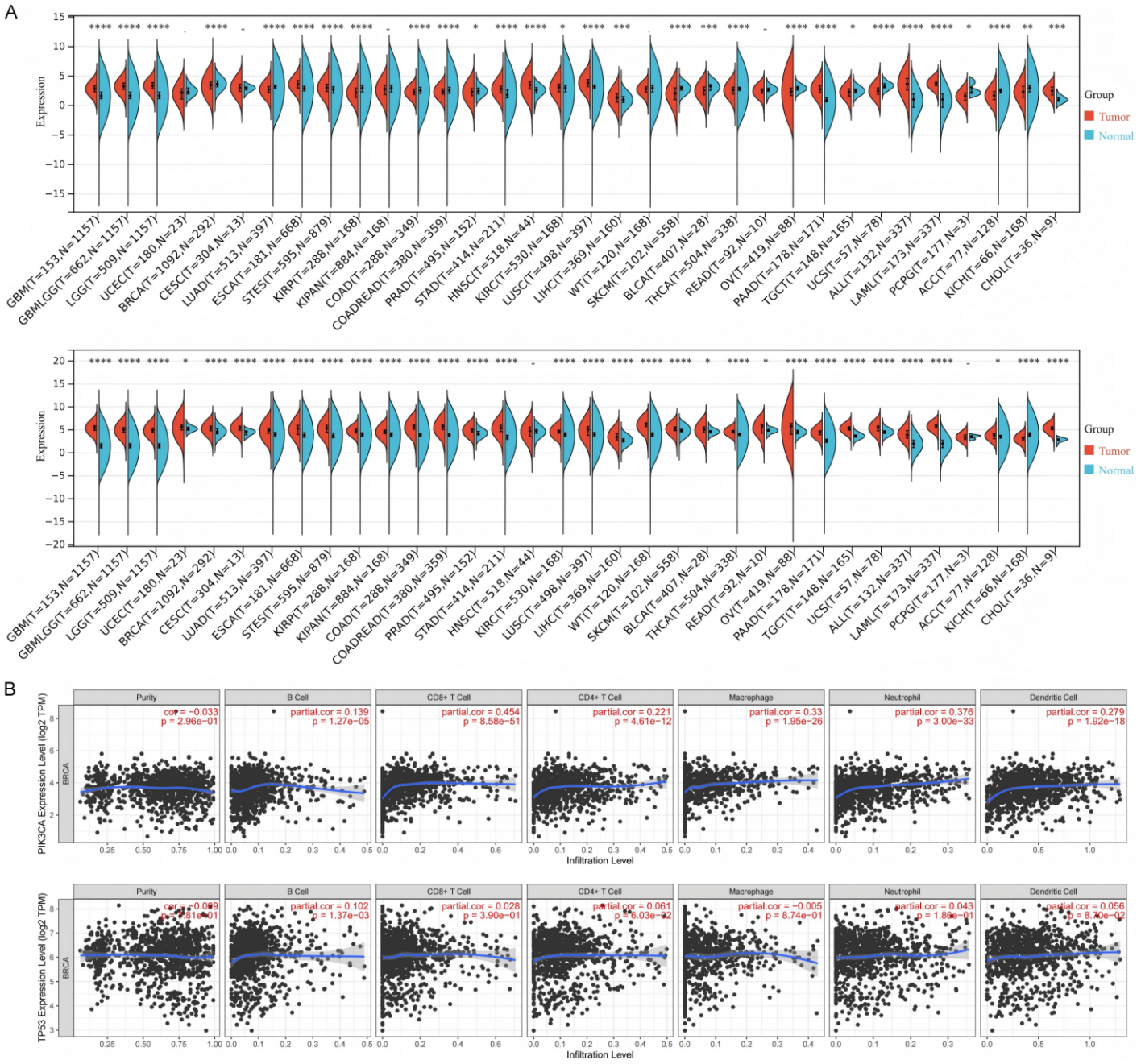
A
Expression
Group
Tumor
Normal
GBM(T=153,N=1157)
GBMLGG(T=662,N=1157)
LGG(T=509,N=1157)
UCEC(T=180,N=23)
BRCA(T=1092,N=292)
CESC(T=304,N=13)
LUAD(T=513,N=397)
ESCA(T=181,N=668)
STES(T=595,N=879)
KIRP(T=288,N=168)
KIPAN(T=884,N=168)
COAD(T=288,N=349)
COADREAD(T=380,N=359)
PRAD(T=495,N=152)
STAD(T=414,N=211)
HNSC(T=518,N=44)
KIRC(T=530,N=168)
LUSC(T=498,N=397)
LIHC(T=369,N=160)
WT(T=120,N=168)
SKCM(T=102,N=558)
BLCA(T=407,N=28)
THCA(T=504,N=338)
READ(T=92,N=10)
OV(T=419,N=88)
PAAD(T=178,N=171)
TGCT(T=148,N=165)
UCS(T=57,N=78)
ALL(T=132,N=337)
LAML(T=173,N=337)
PCPG(T=177,N=3)
ACC(T=77,N=128)
KICH(T=66,N=168)
CHOL(T=36,N=9)
B
Purity
B Cell
CD8+ T Cell
CD4+ T Cell
Macrophage
Neutrophil
Dendritic Cell
PIK3CA Expression Level (log2 TPM)
TP53 Expression Level (log2 TPM)
BRCA
Infiltration Level

Figure 1. Clinical expression and immunomodulatory effects of PIK3CA and TP53 based on online database analysis. A. Pan-cancer expression analysis of PIK3CA and TP53, with emphasis on their upregulated expression in breast cancer. B. Correlations between PIK3CA/TP53 expression and tumor-infiltrating immune cells in breast cancer based on TIMER analysis.

quency was <5. The coexistence or mutual exclusivity of archived PIK3CA and TP53 mutation status was evaluated using the Pearson χ^2 test, and the Spearman rank correlation coefficient was calculated simultaneously to clarify the direction of association. For 4×2 contingency tables containing sparse cells, Fisher-Freeman-Halton exact *P* values with Monte Carlo estimation were used. To address potential confounding by molecular subtype, associations between each gene's mutation status and the seven binary ultrasonographic features included in the composite phenotype score were re-evaluated using Cochran-Mantel-Haenszel tests stratified by molecular subtype, with Holm adjustment across the seven imaging outcomes. The association between the four combined PIK3CA/TP53 mutation patterns and the ordinal composite phenotype score was additionally examined using ordinal logistic regression adjusted for molecular subtype. Spearman correlation was used to examine crude associations between continuous tumor mRNA expression and the composite phenotype score, Partial Spearman correlation adjusted for molecular subtype and both PIK3CA and TP53 mutation status was performed to determine whether any expression-phenotype association was independent of the categorical mutation patterns. Among the 201 patients ultimately included, there were no missing data for the core observation indicators; therefore, the full dataset was analyzed without imputation for missing values.

Results

Online analysis of PIK3CA and TP53 expression

Using online databases, we performed a pan-cancer analysis of PIK3CA and TP53 expression and found that both genes were aberrantly expressed in multiple tumor types. In BC, both genes were also clearly upregulated (**Figure 1A**). TIMER analysis showed no obvious correlation between PIK3CA or TP53 and immune cell infiltration in patients with BC (**Figure 1B**). In the prognostic analysis, PIK3CA expression was significantly associated with BC prognosis (P=0.01), whereas TP53 showed only a borderline effect (P=0.07, **Figure 2A**). However, when survival analysis was further performed specifically in patients with BC, those with high expression of either PIK3CA or TP53 had lower overall survival than those with low expression (**Figure 2B**).

Clinicopathological baseline characteristics of the enrolled patients with BC

Among the 201 patients with primary BC included in this study, the mean age was 53.66±7.86 years; 93 patients (46.3%) were premenopausal and 108 (53.7%) were postmenopausal. Immunohistochemical analysis showed that the percentages of ER-positive, PR-positive, and HER2-positive patients were 68.7%, 59.7%, and 31.3%, respectively, and the mean Ki-67 index was 35.51±17.58%. Luminal tumors predominated among the molecular subtypes, with Luminal A and Luminal B accounting for 32.8% and 40.3%, respectively, whereas HER2-overexpressing and triple-negative BC accounted for 14.9% and 11.9%, respectively (**Table 2**).

Archived PIK3CA and TP53 mutation profiles in BC tissues

Stratified by overall mutation pattern, the PIK3CA/TP53 double-wild-type subgroup accounted for 41.8% (84/201), whereas the proportions of PIK3CA-only mutant, TP53-only mutant, and double-mutant cases were 29.9% (60/201), 22.4% (45/201), and 6.0% (12/201), respectively. Because the double-mutant subgroup contained only 12 patients, all estimates for this subgroup should be interpreted with caution due to the small sample size. Analysis of hotspot mutation sites showed that H1047R was the most frequent PIK3CA mutation, accounting for 45.8% of PIK3CA mutations, followed by E545K (25.0%) and E542K (16.7%). For TP53, the major hotspot mutations were R175H (26.3%), R273H (21.1%), and G245S (15.8%), while mutations at other reported

A

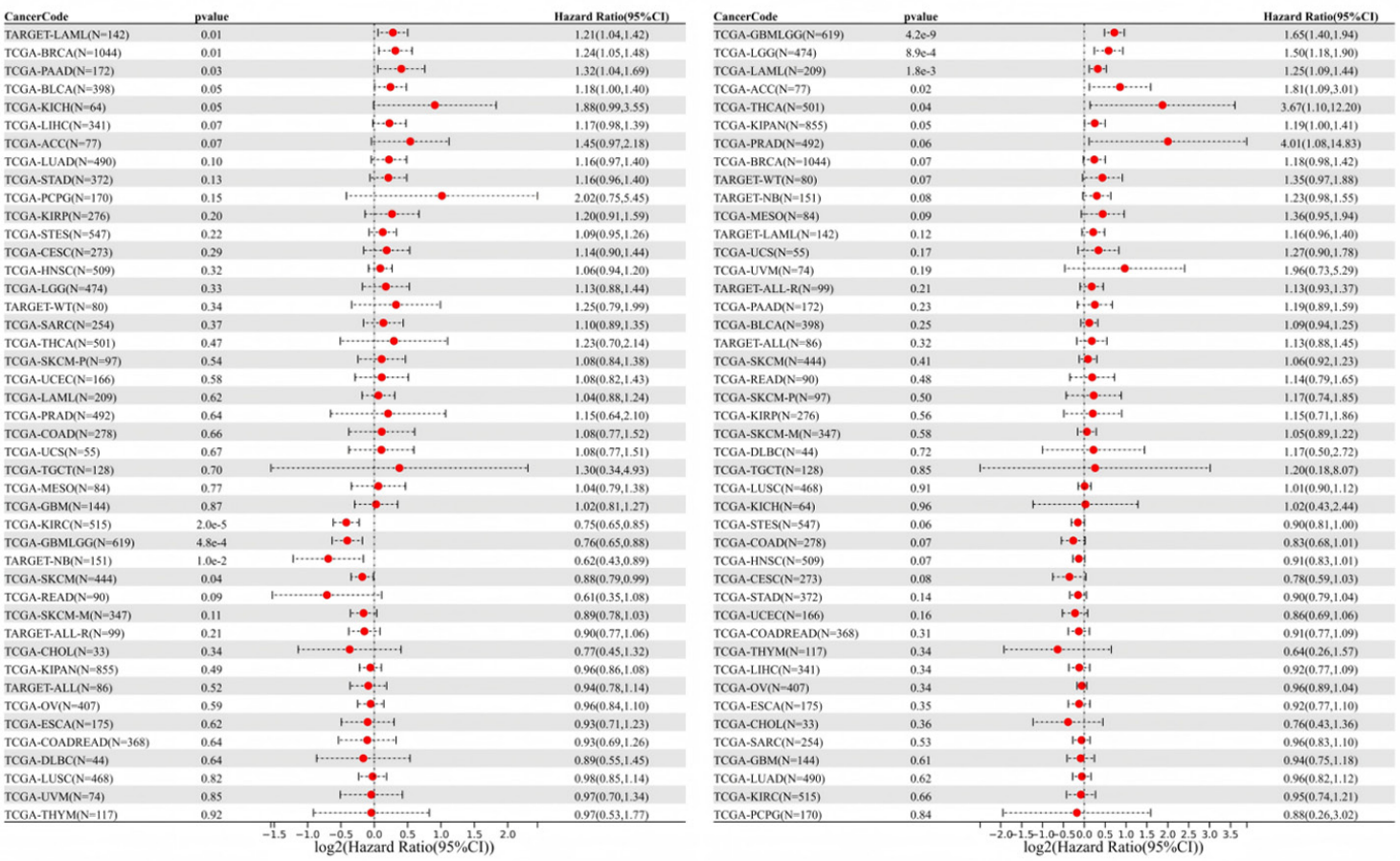
CancerCode
pvalue
Hazard Ratio(95%CI)
TARGET-LAML(N=142) 0.01 1.21(1.04,1.42)
TCGA-BRCA(N=1044) 0.01 1.24(1.05,1.48)
TCGA-PAAD(N=172) 0.03 1.32(1.04,1.69)
TCGA-BLCA(N=398) 0.05 1.18(1.00,1.40)
TCGA-KICH(N=64) 0.05 1.88(0.99,3.55)
TCGA-LIHC(N=341) 0.07 1.17(0.98,1.39)
TCGA-ACC(N=77) 0.07 1.45(0.97,2.18)
TCGA-LUAD(N=490) 0.10 1.16(0.97,1.40)
TCGA-STAD(N=372) 0.13 1.16(0.96,1.40)
TCGA-PCPG(N=170) 0.15 2.02(0.75,5.45)
TCGA-KIRP(N=276) 0.20 1.20(0.91,1.59)
TCGA-STES(N=547) 0.22 1.09(0.95,1.26)
TCGA-CESC(N=273) 0.29 1.14(0.90,1.44)
TCGA-HNSC(N=509) 0.32 1.06(0.94,1.20)
TCGA-LGG(N=474) 0.33 1.13(0.88,1.44)
TARGET-WT(N=80) 0.34 1.25(0.79,1.99)
TCGA-SARC(N=254) 0.37 1.10(0.89,1.35)
TCGA-THCA(N=501) 0.47 1.23(0.70,2.14)
TCGA-SKCM-P(N=97) 0.54 1.08(0.84,1.38)
TCGA-UCEC(N=166) 0.58 1.08(0.82,1.43)
TCGA-LAML(N=209) 0.62 1.04(0.88,1.24)
TCGA-PRAD(N=492) 0.64 1.15(0.64,2.10)
TCGA-COAD(N=278) 0.66 1.08(0.77,1.52)
TCGA-UCS(N=55) 0.67 1.08(0.77,1.51)
TCGA-TGCT(N=128) 0.70 1.30(0.34,4.93)
TCGA-MESO(N=84) 0.77 1.04(0.79,1.38)
TCGA-GBM(N=144) 0.87 1.02(0.81,1.27)
TCGA-KIRC(N=515) 2.0e-5 0.75(0.65,0.85)
TCGA-GBMLGG(N=619) 4.8e-4 0.76(0.65,0.88)
TARGET-NB(N=151) 1.0e-2 0.62(0.43,0.89)
TCGA-SKCM(N=444) 0.04 0.88(0.79,0.99)
TCGA-READ(N=90) 0.09 0.61(0.35,1.08)
TCGA-SKCM-M(N=347) 0.11 0.89(0.78,1.03)
TARGET-ALL-R(N=99) 0.21 0.90(0.77,1.06)
TCGA-CHOL(N=33) 0.34 0.77(0.45,1.32)
TCGA-KIPAN(N=855) 0.49 0.96(0.86,1.08)
TARGET-ALL(N=86) 0.52 0.94(0.78,1.14)
TCGA-OV(N=407) 0.59 0.96(0.84,1.10)
TCGA-ESCA(N=175) 0.62 0.93(0.71,1.23)
TCGA-COADREAD(N=368) 0.64 0.93(0.69,1.26)
TCGA-DLBC(N=44) 0.64 0.89(0.55,1.45)
TCGA-LUSC(N=468) 0.82 0.98(0.85,1.14)
TCGA-UVM(N=74) 0.85 0.97(0.70,1.34)
TCGA-THYM(N=117) 0.92 0.97(0.53,1.77)
−1.5 −1.0 −0.5 0.0 0.5 1.0 1.5 2.0
log2(Hazard Ratio(95%CI))
CancerCode
pvalue
Hazard Ratio(95%CI)
TCGA-GBMLGG(N=619) 4.2e-9 1.65(1.40,1.94)
TCGA-LGG(N=474) 8.9e-4 1.50(1.18,1.90)
TCGA-LAML(N=209) 1.8e-3 1.25(1.09,1.44)
TCGA-ACC(N=77) 0.02 1.81(1.09,3.01)
TCGA-THCA(N=501) 0.04 3.67(1.10,12.20)
TCGA-KIPAN(N=855) 0.05 1.19(1.00,1.41)
TCGA-PRAD(N=492) 0.06 4.01(1.08,14.83)
TCGA-BRCA(N=1044) 0.07 1.18(0.98,1.42)
TARGET-WT(N=80) 0.07 1.35(0.97,1.88)
TARGET-NB(N=151) 0.08 1.23(0.98,1.55)
TCGA-MESO(N=84) 0.09 1.36(0.95,1.94)
TARGET-LAML(N=142) 0.12 1.16(0.96,1.40)
TCGA-UCS(N=55) 0.17 1.27(0.90,1.78)
TCGA-UVM(N=74) 0.19 1.96(0.73,5.29)
TARGET-ALL-R(N=99) 0.21 1.13(0.93,1.37)
TCGA-PAAD(N=172) 0.23 1.19(0.89,1.59)
TCGA-BLCA(N=398) 0.25 1.09(0.94,1.25)
TARGET-ALL(N=86) 0.32 1.13(0.88,1.45)
TCGA-SKCM(N=444) 0.41 1.06(0.92,1.23)
TCGA-READ(N=90) 0.48 1.14(0.79,1.65)
TCGA-SKCM-P(N=97) 0.50 1.17(0.74,1.85)
TCGA-KIRP(N=276) 0.56 1.15(0.71,1.86)
TCGA-SKCM-M(N=347) 0.58 1.05(0.89,1.22)
TCGA-DLBC(N=44) 0.72 1.17(0.50,2.72)
TCGA-TGCT(N=128) 0.85 1.20(0.18,8.07)
TCGA-LUSC(N=468) 0.91 1.01(0.90,1.12)
TCGA-KICH(N=64) 0.96 1.02(0.43,2.44)
TCGA-STES(N=547) 0.06 0.90(0.81,1.00)
TCGA-COAD(N=278) 0.07 0.83(0.68,1.01)
TCGA-HNSC(N=509) 0.07 0.91(0.83,1.01)
TCGA-CESC(N=273) 0.08 0.78(0.59,1.03)
TCGA-STAD(N=372) 0.14 0.90(0.79,1.04)
TCGA-UCEC(N=166) 0.16 0.86(0.69,1.06)
TCGA-COADREAD(N=368) 0.31 0.91(0.77,1.09)
TCGA-THYM(N=117) 0.34 0.64(0.26,1.57)
TCGA-LIHC(N=341) 0.34 0.92(0.77,1.09)
TCGA-OV(N=407) 0.34 0.96(0.89,1.04)
TCGA-ESCA(N=175) 0.35 0.92(0.77,1.10)
TCGA-CHOL(N=33) 0.36 0.76(0.43,1.36)
TCGA-SARC(N=254) 0.53 0.96(0.83,1.10)
TCGA-GBM(N=144) 0.61 0.94(0.75,1.18)
TCGA-LUAD(N=490) 0.62 0.96(0.82,1.12)
TCGA-KIRC(N=515) 0.66 0.95(0.74,1.21)
TCGA-PCPG(N=170) 0.84 0.88(0.26,3.02)
−2.0 −1.5 −1.0 −0.5 0.0 0.5 1.0 1.5 2.0 2.5 3.0 3.5
log2(Hazard Ratio(95%CI))

B

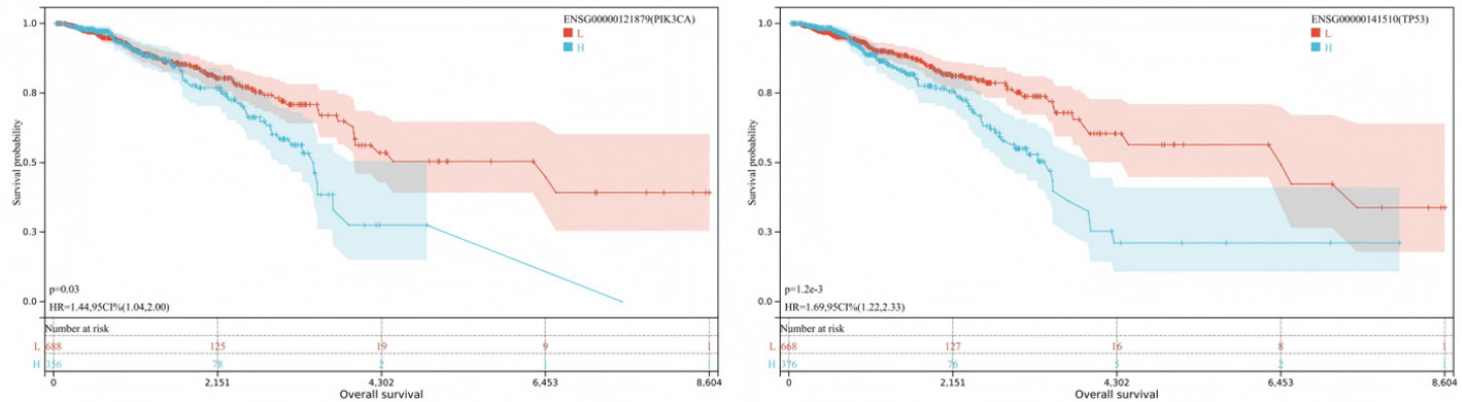
ENSG00000121879(PIK3CA)
L
H
Survival probability
p=0.03
HR=1.44,95CI%(1.04,2.00)
Number at risk
L 688 125 19 9 1
H 356 76 5 1
0 2,151 4,302 6,453 8,604
Overall survival
ENSG00000141510(TP53)
L
H
Survival probability
p=1.2e-3
HR=1.69,95CI%(1.22,2.33)
Number at risk
L 668 127 16 8 1
H 376 76 4 1
0 2,151 4,302 6,453 8,604
Overall survival

Figure 2. Prognostic impact of PIK3CA and TP53 based on online database analysis. A. Kaplan-Meier analysis of the prognostic significance of PIK3CA and TP53 expression in breast cancer. B. Overall survival comparison between high- and low-expression groups of PIK3CA and TP53 in breast cancer.

Table 2. Clinicopathological baseline characteristics of the enrolled patients with primary breast cancer

Feature category	Specific subgroup	Total population (n=201)
Demographic characteristics	Age	53.66±7.86
	Menopausal status, n (%)	
	Premenopausal	93 (46.3%)
	Postmenopausal	108 (53.7%)
Histopathological characteristics	Histological grade, n (%)	
	Grade I	24 (11.9%)
	Grade II	111 (55.2%)
	Grade III	66 (32.8%)
	T stage, n (%)	
	T1	87 (43.3%)
	T2	93 (46.3%)
	T3-T4	21 (10.4%)
	N stage, n (%)	
	N0	114 (56.7%)
	N1-N3	87 (43.3%)
	Molecular subtype, n (%)	
	Luminal A	66 (32.8%)
	Luminal B	81 (40.3%)
	HER2 overexpression	30 (14.9%)
	Triple-negative BC	24 (11.9%)
Immunohistochemical characteristics	ER expression, n (%)	
	Positive	138 (68.7%)
	Negative	63 (31.3%)
	PR expression, n (%)	
	Positive	120 (59.7%)
	Negative	81 (40.3%)
	HER2 expression, n (%)	
	Positive	63 (31.3%)
	Negative	138 (68.7%)
	Ki-67 index (%)	35.51±17.58

sites accounted for 36.8% of all TP53 mutations (**Table 3**).

Correlation between archived PIK3CA mutation status and multidimensional ultrasound features of BC

Comparative analysis of ultrasound features between patients with wild-type PIK3CA (n=129) and mutant PIK3CA (n=72) showed no statistically significant differences in lesion size, internal echogenicity or aspect ratio (P>0.05). Differences did emerge, however, in several other sonographic features. Patients with PIK3CA mutation showed lower proportions of irregular lesion shape, spiculated margins, microcalcification, posterior acoustic attenuation, and Adler blood-flow grade II-III than those with wild-type PIK3CA (P=0.017 for posterior acoustic attenuation and P<0.001 for the remaining features) (**Table 4**).

Table 3. Mutation profiles of PIK3CA and TP53 in breast cancer tissues

Mutation category	Specific subgroup/site	Number of cases (n)	Mutation frequency/site proportion (%)
Stratification of overall mutation status	PIK3CA-TP53 double wild type	84	41.8%
	PIK3CA-only mutant type	60	29.9%
	TP53-only mutant type	45	22.4%
	PIK3CA-TP53 double mutant type	12	6.0%
Total PIK3CA mutations	-	72	35.8% (overall mutation rate in the total population)
Distribution of PIK3CA hotspot mutation sites	H1047R	33	45.8% (proportion of total mutations)
	E545K	18	25.0% (proportion of total mutations)
	E542K	12	16.7% (proportion of total mutations)
	Other reported sites	9	12.5% (proportion of total mutations)
Total TP53 mutations	-	57	28.4 (overall mutation rate in the total population)
Distribution of TP53 hotspot mutation sites	R175H	15	26.3% (proportion of total mutations)
	R273H	12	21.1% (proportion of total mutations)
	G245S	9	15.8% (proportion of total mutations)
	Other reported sites	21	36.8% (proportion of total mutations)

Table 4. Associations between PIK3CA mutation status and multidimensional ultrasonographic features of breast cancer

Ultrasound feature category	Specific subgroup	PIK3CA wild type (n=129)	PIK3CA mutant type (n=72)	χ^2	P
Lesion size	≤2 cm	63 (48.8%)	30 (41.7%)	0.965	0.617
	2-5 cm	57 (44.2%)	36 (50.0%)		
	>5 cm	9 (7.0%)	6 (8.3%)		
Lesion shape	Regular	24 (18.6%)	33 (45.8%)	16.861	<0.001
	Irregular	105 (81.4%)	39 (54.2%)		
Lesion margin	Clear/indistinct	39 (30.2%)	39 (54.2%)	11.152	<0.001
	Spiculated	90 (69.8%)	33 (45.8%)		
Internal echogenicity	Homogeneous	33 (25.6%)	27 (37.5%)	3.135	0.077
	Heterogeneous	96 (74.4%)	45 (62.5%)		
Microcalcification	Absent	57 (44.2%)	51 (70.8%)	13.204	<0.001
	Present	72 (55.8%)	21 (29.2%)		
Posterior acoustic features	No change/enhancement	75 (58.1%)	54 (75.0%)	5.714	0.017
	Attenuation	54 (41.9%)	18 (25.0%)		
Aspect ratio	<1	66 (51.2%)	42 (58.3%)	0.956	0.328
	≥1	63 (48.8%)	30 (41.7%)		
Adler blood flow grade	Grade 0-I	42 (32.6%)	45 (62.5%)	16.881	<0.001
	Grade II-III	87 (67.4%)	27 (37.5%)		

Table 5. Associations between TP53 mutation status and multidimensional ultrasonographic features of breast cancer

Ultrasound feature category	Specific subgroup	TP53 wild type (n=144)	TP53 mutant type (n=57)	χ^2	P
Lesion size	≤2 cm	72 (50.0%)	21 (36.8%)	3.225	0.200
	2-5 cm	63 (43.8%)	30 (52.6%)		
	>5 cm	9 (6.2%)	6 (10.5%)		
Lesion shape	Regular	57 (39.6%)	0 (0.0%)	31.492	<0.001
	Irregular	87 (60.4%)	57 (100.0%)		
Lesion margin	Clear/indistinct	72 (50.0%)	6 (10.5%)	26.793	<0.001
	Spiculated	72 (50.0%)	51 (89.5%)		
Internal echogenicity	Homogeneous	54 (37.5%)	6 (10.5%)	14.190	<0.001
	Heterogeneous	90 (62.5%)	51 (89.5%)		
Microcalcification	Absent	87 (60.4%)	21 (36.8%)	9.129	0.003
	Present	57 (39.6%)	36 (63.2%)		
Posterior acoustic features	No change/enhancement	96 (66.7%)	33 (57.9%)	1.367	0.242
	Attenuation	48 (33.3%)	24 (42.1%)		
Aspect ratio	<1	93 (64.6%)	15 (26.3%)	24.050	<0.001
	≥1	51 (35.4%)	42 (73.7%)		
Adler blood flow grade	Grade 0-I	72 (50.0%)	15 (26.3%)	9.331	0.002
	Grade II-III	72 (50.0%)	42 (73.7%)		

Correlation between archived TP53 mutation status and multidimensional ultrasound features of BC

Compared with patients with wild-type TP53 (n=144), those with TP53 mutation (n=57) showed higher proportions of irregular lesion shape, spiculated margins, heterogeneous internal echogenicity, microcalcification, aspect ratio ≥1, and Adler blood-flow grade II-III (P=0.003 for microcalcification, P=0.002 for Adler blood-flow grade, and P<0.001 for the

Table 6. Cross-tabulation of PIK3CA and TP53 mutation status in breast cancer tissues

Group	TP53 wild type	TP53 mutant type	Total	χ^2	P	r
PIK3CA wild type	84	45	129	7.548	0.006	-0.194
PIK3CA mutant type	60	12	72			
Total	144	57	201			

Table 7. Clinicopathological and molecular characteristics according to combined PIK3CA/TP53 mutation patterns in breast cancer

Projects	Double WT (n=84)	PIK3CA-only mutant (n=60)	TP53-only mutant (n=45)	Double mutant (n=12)	Statistic	P
Age (years)	54.00±7.29	54.20±8.18	53.38±8.27	49.58±8.39	F=1.245	0.295
Premenopausal (n; %)	42 (50.0%)	27 (45.0%)	21 (46.7%)	3 (25.0%)	χ^2=2.696	0.441
Postmenopausal (n; %)	42 (50.0%)	33 (55.0%)	24 (53.3%)	9 (75.0%)		
Grade III (n; %)	30 (35.7%)	15 (25.0%)	15 (33.3%)	6 (50.0%)	χ^2=3.594	0.309
T3-T4 stage (n; %)	9 (10.7%)	3 (5.0%)	9 (20.0%)	0 (0.0%)	χ^2=7.698	0.053
N1-N3 stage (n; %)	27 (32.1%)	30 (50.0%)	24 (53.3%)	6 (50.0%)	χ^2=7.421	0.060
Luminal A (n; %)	33 (39.3%)	18 (30.0%)	12 (26.7%)	3 (25.0%)	χ^2=18.503	0.030
Luminal B (n; %)	24 (28.6%)	24 (40.0%)	27 (60.0%)	6 (50.0%)		
HER2-overexpressing (n; %)	12 (14.3%)	12 (20.0%)	3 (6.7%)	3 (25.0%)		
Triple-negative (n; %)	15 (17.9%)	6 (10.0%)	3 (6.7%)	0 (0.0%)		
ER positive (n; %)	51 (60.7%)	42 (70.0%)	36 (80.0%)	9 (75.0%)	χ^2=5.428	0.143
PR positive (n; %)	48 (57.1%)	33 (55.0%)	33 (73.3%)	6 (50.0%)	χ^2=4.725	0.193
HER2 positive (n; %)	30 (35.7%)	18 (30.0%)	9 (20.0%)	6 (50.0%)	χ^2=5.428	0.143
Ki-67 index (%)	34.85±16.27	35.77±19.35	35.44±16.44	39.03±22.67	F=0.202	0.895
Cancer PIK3CA mRNA	2.51 (2.36, 2.65)	4.74 (4.37, 5.15)	2.53 (2.43, 2.65)	3.89 (3.79, 4.37)	H=140.089	<0.001
Cancer TP53 mRNA	2.35 (2.27, 2.44)	2.33 (2.23, 2.42)	4.48 (3.24, 4.79)	4.11 (3.84, 4.19)	H=105.005	<0.001

Note: The double-mutant subgroup included only 12 patients; estimates for this subgroup are exploratory and should not be interpreted as confirmatory evidence.

remaining features). No statistically significant differences were observed between the two groups only for lesion size and posterior acoustic features (P>0.05) (**Table 5**).

Coexistence and mutual exclusivity of archived PIK3CA and TP53 mutation status

Among 201 patients, 41.8% (84/201) harbored both PIK3CA and TP53 wild type; 6.0% (12/201) patients carried both PIK3CA and TP53 mutant types. Analysis of the mutation patterns of PIK3CA and TP53 showed a statistically significant association between the two genes (P=0.006). Further Spearman rank correlation analysis yielded r=-0.194, indicating that the mutation statuses of the two genes were related in this cohort (**Table 6**).

Combined archived PIK3CA/TP53 mutation patterns and clinicopathological features

Patients were divided into four groups according to combined PIK3CA/TP53 mutation status: Age, menopausal status, histological grade, T stage, N stage, ER, PR, HER2 status, and Ki-67 index did not differ significantly among the four groups (P>0.05), however, molecular subtype distribution differed significantly (P= 0.030). In addition, PIK3CA mRNA expression was higher in groups with PIK3CA mutation, whereas TP53 mRNA expression was higher in groups with TP53 mutation (both P<0.001), indicating distinct molecular characteristics across mutation-pattern groups (**Table 7**).

Combined archived PIK3CA/TP53 mutation patterns and ultrasonographic phenotypes

Multidimensional ultrasonographic features differed significantly among the four combined mutation-pattern groups, significant differences were observed in lesion size >2 cm, irregular shape, spiculated margin, heterogeneous echogenicity, microcalcification, aspect ratio ≥1, and Adler blood-flow grade II-III (P<0.05), whereas posterior acoustic attenuation showed no significant difference (P=0.093). Descrip-

Table 8. Multidimensional ultrasonographic phenotypes according to combined PIK3CA/TP53 mutation patterns in breast cancer

Projects	Double WT (n=84)	PIK3CA-only mutant (n=60)	TP53-only mutant (n=45)	Double mutant (n=12)	Statistic	P
Lesion size >2 cm	42 (50.0%)	30 (50.0%)	24 (53.3%)	12 (100.0%)	χ^2=11.143	0.011
Irregular shape	60 (71.4%)	27 (45.0%)	45 (100.0%)	12 (100.0%)	χ^2=43.526	<0.001
Spiculated margin	51 (60.7%)	21 (35.0%)	39 (86.7%)	12 (100.0%)	χ^2=37.250	<0.001
Heterogeneous echogenicity	57 (67.9%)	33 (55.0%)	39 (86.7%)	12 (100.0%)	χ^2=17.756	<0.001
Microcalcification	39 (46.4%)	18 (30.0%)	33 (73.3%)	3 (25.0%)	χ^2=21.831	<0.001
Posterior acoustic attenuation	33 (39.3%)	15 (25.0%)	21 (46.7%)	3 (25.0%)	χ^2=6.408	0.095
Aspect ratio ≥1	33 (39.3%)	18 (30.0%)	30 (66.7%)	12 (100.0%)	χ^2=29.502	<0.001
Adler grade II-III	48 (57.1%)	24 (40.0%)	39 (86.7%)	3 (25.0%)	χ^2=28.196	<0.001
Malignant ultrasound phenotype score, median (IQR)	4.00 (3.00, 5.00)	3.00 (2.00, 3.00)	6.00 (5.00, 6.00)	4.50 (4.00, 5.25)	H=90.814	<0.001
Score ≥4	48 (57.1%)	12 (20.0%)	45 (100.0%)	12 (100.0%)	χ^2=76.971	<0.001

Note: The exploratory composite ultrasound phenotype score ranged from 0 to 7. One point was assigned for each of the following features: irregular shape, spiculated margin, heterogeneous echogenicity, microcalcification, posterior acoustic attenuation, aspect ratio ≥1, and Adler blood-flow grade II-III. WT, wild type; IQR, interquartile range. This unweighted score was used as an exploratory index of phenotype burden and has not been externally validated as a diagnostic scale. The double-mutant subgroup included only 12 patients; estimates for this subgroup are exploratory and should not be interpreted as confirmatory evidence.

tively, the PIK3CA-only mutant group had the lowest median composite phenotype score, whereas the TP53-only mutant group had the highest; inferential interpretation was based on the subtype-adjusted ordinal model rather than on unadjusted pairwise comparisons (**Table 8**).

Interobserver and intraobserver reproducibility

Interobserver agreement ranged from 80.5% to 95.1%, with kappa coefficients ranging from 0.608 to 0.901. Intraobserver agreement ranged from 87.8% to 97.6%, with kappa coefficients ranging from 0.752 to 0.942. The lowest interobserver coefficients were observed for microcalcification and internal echogenicity, whereas the highest interobserver coefficient was observed for the aspect-ratio category. Feature-specific coefficients and their 95% confidence intervals are presented in Supplementary Table 2.

Molecular subtype-adjusted analyses

After stratification by molecular subtype and Holm adjustment, PIK3CA mutation remained associated with lower frequencies of irregular shape, spiculated margin, microcalcification, posterior acoustic attenuation, and Adler blood-flow grade II-III. TP53 mutation remained associated with irregular shape, spiculated margin, heterogeneous echogenicity, microcalcification, aspect ratio ≥1, and Adler blood-flow grade II-III. In the subtype-adjusted ordinal logistic model, the combined mutation pattern remained associated with the composite phenotype score (global P<0.001). Relative to the double-wild-type group, the PIK3CA-only mutant group had lower odds of being in a higher score category (OR=0.17, 95% CI 0.09-0.33, Holm-adjusted P<0.001), whereas the TP53-only mutant group had higher odds (OR=13.23, 95% CI 6.09-28.72, Holm-adjusted P<0.001). The estimate for the double-mutant group was exploratory because of its small sample size (OR=3.48, 95% CI 1.21-9.99, Holm-adjusted P=0.020, Supplementary Table 1).

Differences in PIK3CA and TP53 mRNA expression between BC tissues and matched adjacent normal tissues

qRT-PCR results showed that the mRNA expression levels of PIK3CA and TP53 were higher in BC tissues than in matched adjacent normal breast tissues (P<0.001) (**Figure 3A**). Stratified analysis further showed that the relative PIK3CA mRNA expression level in cancer tissues from patients with PIK3CA mutation was higher than that in patients with wild-type PIK3CA (P<0.05), and TP53 mRNA expression was likewise higher in TP53-mutant tumors than in TP53-wild-type tumors (P<0.05) (**Figure 3B**). Moreover, mRNA expression levels differed across reported mutation-site categories in both genes. Among PIK3CA mutation-positive tumors, the H1047R category showed the most marked upregulation (P<0.05), whereas among TP53 mutation-positive tumors, the highest expression level was observed in the R175H category (P<0.05, **Figure 3C**).

Continuous associations between gene expression and ultrasonographic phenotype burden

PIK3CA mRNA expression was inversely correlated with the composite ultrasonographic phenotype score in the crude analysis (r_s=-0.369, P<0.001), whereas TP53 mRNA expression was positively correlated with the score (r_s=0.459, P<0.001). However, neither association remained significant after adjustment for molecular subtype and both PIK3CA and TP53 mutation status (partial r_s=0.020, P=0.776 for PIK3CA; partial r_s=0.055, P=0.435 for TP53).

Discussion

In this study, we initially leveraged online public databases to characterize the expression patterns and prognostic value of PIK3CA and TP53 in BC, and then performed a retrospective analysis in 201 patients with primary BC to evaluate archived PIK3CA/TP53 mutation results, transcriptional abnormalities, and their associations with multidimensional ultrasonographic phenotypes of BC. Several findings stood out in this cohort. PIK3CA and TP53 were highly expressed in BC, and their archived mutation patterns were statistically related. More importantly, the two genes were linked to clearly different ultrasound phenotypes. PIK3CA mutation was associated with less aggressive sonographic features, whereas TP53 mutation was more often seen in lesions with malignant-appearing ultrasound findings.

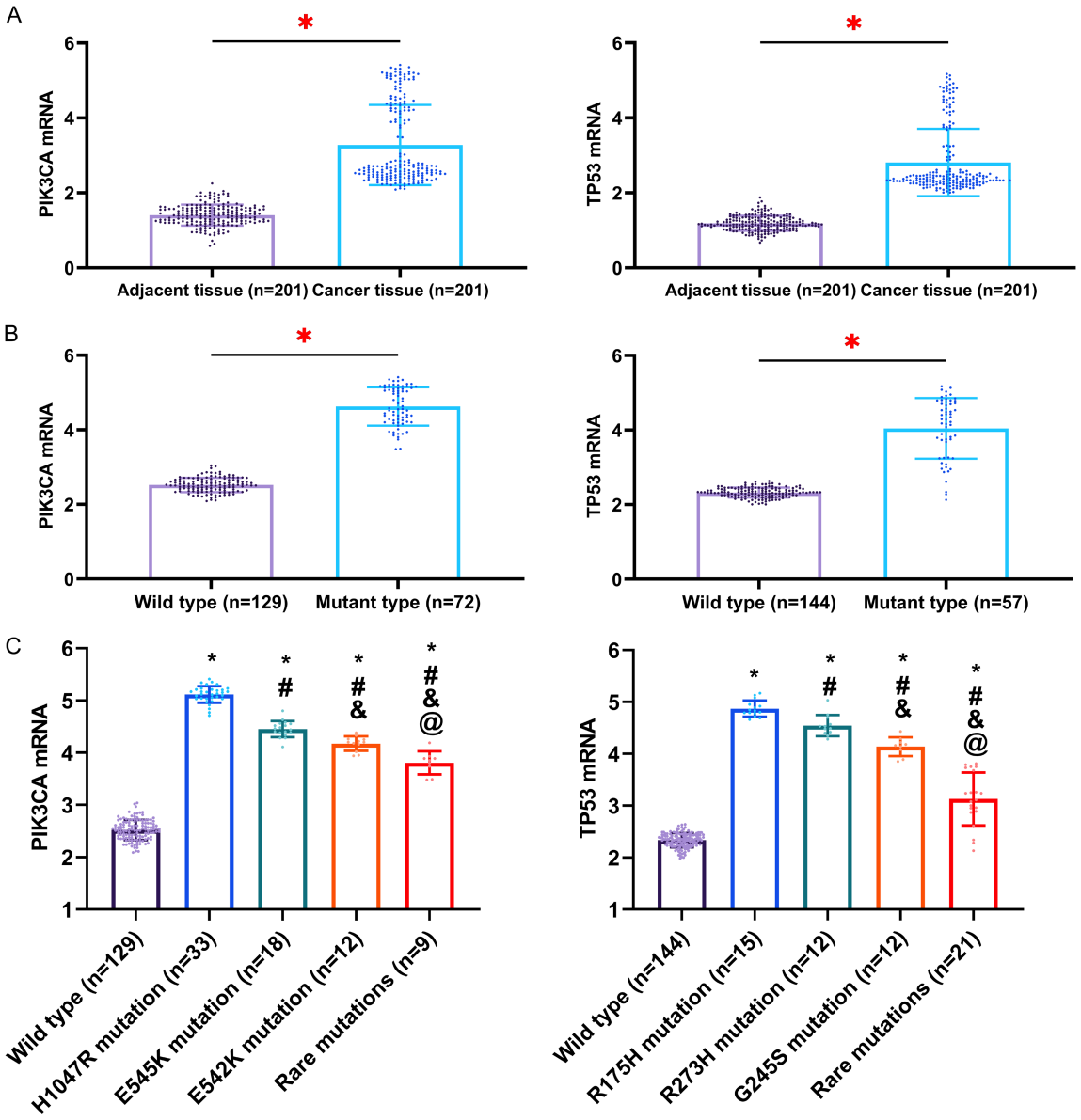

Figure 3. mRNA expression patterns of PIK3CA and TP53 in breast cancer tissues and matched adjacent normal tissues. (A) Relative mRNA expression levels of PIK3CA and TP53 in breast cancer tissues and matched adjacent normal tissues. *P<0.05. (B) Comparison of PIK3CA and TP53 mRNA expression between mutant and wild-type tumors. *P<0.05. (C) Relative mRNA expression of PIK3CA and TP53 according to reported mutation-site categories derived from archived molecular testing records. For (C), the global Kruskal-Wallis tests were significant for both genes (both P<0.001), and pairwise *P* values were adjusted using Holm's method. *P_adj<0.05 versus wild type; #P_adj<0.05 versus H1047R/R175H; &P_adj<0.05 versus E545K/R273H; and @P_adj<0.05 versus E542K/G245S. All indicated pairwise comparisons remained significant after adjustment (all P_adj<0.001).

Bioinformatic analyses from public databases confirmed dysregulated expression of PIK3CA and TP53 in multiple malignant tumors, with both genes being highly expressed in BC. Prognostic analysis further suggested that high expression of these two genes was associated with poorer overall survival, with the association being more evident for PIK3CA, while TP53 showed only a borderline effect. TIMER analysis did not reveal any clear relationship between gene expression and immune cell infiltration in BC. Overall, these results support the importance of PIK3CA and TP53 in BC and provide a biological rationale for the subsequent analysis of our clinical samples.

Among the 201 patients enrolled in this study, the overall mutation rates of PIK3CA and TP53 were 35.8% and 28.4%, respectively, which are fully consistent with the mutation ranges of 30%-40% and 20%-35% reported in previous BC genomic studies [14, 15]. The observed mutation frequencies are consistent with those reported in prior BC genomic studies. We also found that the mutation states of these two genes were statistically associated. One possible explanation is that the two genes regulate two major pathways involved in the malignant transformation of mammary epithelial cells. Gain-of-function mutations in PIK3CA directly activate the PI3K/AKT pathway, driving abnormal proliferation and resistance to apoptosis [16]. In contrast, inactivating mutations in TP53 disrupt cell-cycle checkpoints and directly compromise genomic stability [17]. Because their downstream effects may overlap to some extent during tumor clonal evolution, concurrent alterations may fail to confer substantial additional survival benefit on tumor clones and may even promote excessive genomic instability. Related patterns have likewise been reported in TCGA-based BC studies [18, 19], further analysis based on combined PIK3CA/TP53 mutation patterns strengthened this interpretation. Although most clinicopathological variables were comparable among the four mutation-pattern groups, molecular subtype distribution, gene-expression profiles, and ultrasound phenotype burden differed significantly. The principal associations were retained after adjustment or stratification for molecular subtype, indicating that subtype did not fully explain the observed radiogenomic differences; nevertheless, the magnitude of individual associations may vary across subtypes and should not be regarded as uniform. Notably, the PIK3CA-only mutant group showed a lower malignant ultrasound phenotype score, whereas the TP53-only mutant group showed the highest score, these findings suggest that combined mutation status may better reflect radiogenomic heterogeneity than single-gene analysis alone, and may help explain the diversity of ultrasound phenotypes in breast cancer.

Previous studies have mainly examined PIK3CA or TP53 separately or developed mutation-prediction models using conventional ultrasound or radiomic features [11, 12]. Differences in molecular-subtype composition, mutation assays, imaging protocols, and feature definitions may account for the heterogeneity among reported findings. The present study extends this literature by describing the four combined PIK3CA/TP53 mutation patterns and integrating reported hotspot categories with tumor mRNA expression; however, it remains an exploratory association study rather than a validated prediction model.

Our finding that PIK3CA-mutant tumors displayed less aggressive ultrasound features is biologically plausible. This association likely reflects an indirect radiogenomic relationship rather than direct causality. Ultrasound morphology is shaped by multiple factors, including tumor genotype, histological architecture, stromal reaction, angiogenesis, calcification, and molecular subtype. Therefore, the relatively less aggressive ultrasound phenotype observed in PIK3CA-mutant tumors may reflect the combined influence of PIK3CA-related signaling and its clinicopathological background, rather than a direct effect of PIK3CA mutation alone [20, 21]. Clinically, PIK3CA mutations are more frequently enriched in Luminal BC, which usually shows lower-grade malignant behavior and more indolent growth [22]. This pattern is well aligned with the relatively less aggressive ultrasound phenotype observed in the present study, PIK3CA activation is frequently enriched in luminal tumors and may be associated with slower expansile growth and a less pronounced desmoplastic interface, which could plausibly contribute to fewer spiculated margins, microcalcifications, and high-grade vascular signals. Some earlier studies did not detect a significant association, and that inconsistency may largely have resulted from differences in the molecular subtype composition of the study population [23]. If a cohort contains an excessive proportion of triple-negative BC, the true relationship may easily be diluted because PIK3CA mutations are less common in that subtype and its biological behavior is distinct.

In sharp contrast to PIK3CA, TP53 mutation was positively associated with nearly all malignant ultrasonographic signs of BC. In the mutant group, lesions were almost uniformly irregular in shape, and the detection rates of spiculated margins, microcalcifications, aspect ratio ≥1, and high-grade blood flow were all

markedly higher than in the wild-type group. TP53 is widely regarded as the "guardian of the genome", and the most immediate consequence of its functional loss is broad impairment of genomic stability. Loss of p53-mediated genomic surveillance promotes high-grade cellular atypia, infiltrative growth, necrosis, stromal remodeling, and angiogenesis, providing a plausible pathological basis for irregular shape, heterogeneous echogenicity, spiculation, microcalcification, and increased blood-flow signals. However, the present retrospective association cannot establish a direct mechanistic pathway from TP53 mutation to ultrasound morphology [24, 25]. Similar associations between TP53 status and breast ultrasonographic morphology have been reported previously [12]; however, differences in molecular-subtype composition, mutation detection, and imaging methodology preclude direct equivalence between the earlier findings and the present results.

Finally, qRT-PCR analysis of paired samples further confirmed that the mRNA expression levels of PIK3CA and TP53 were higher in BC tissues than in adjacent normal tissues, and that expression levels in mutant tumors exceeded those in wild-type tumors, which was consistent with the earlier bioinformatic findings of upregulated expression. Among hotspot mutations, PIK3CA H1047R and TP53 R175H showed the most pronounced expression increase. This may partly explain why different hotspot mutations correspond to subtle differences in biological behavior and ultrasound phenotype, and it also provides an initial clue for future site-specific mechanistic studies. Although crude expression-phenotype correlations were observed, they disappeared after adjustment for molecular subtype and both mutation statuses, indicating that the apparent gradients were largely explained by the underlying categorical mutation patterns. The present data therefore do not support an independent dose-response relationship between mRNA expression and ultrasonographic phenotype burden.

Still, this study has several limitations. As a single-center retrospective study, the overall sample size was modest, and the double-mutant subgroup contained only 12 patients; estimates for this subgroup were vulnerable to sparse-cell bias and should be regarded as exploratory rather than confirmatory. Larger multicenter cohorts are required to define the ultrasonographic characteristics of double-mutant tumors reliably. In addition, the targeted Sanger assay had limited sensitivity for low-frequency somatic variants and did not assess the complete coding sequences, copy-number alterations, or structural variants; clinically relevant alterations may therefore have been missed, and the reported categories should not be interpreted as comprehensive genomic profiles. The inclusion of only invasive ductal and lobular carcinoma may limit the generalizability of our findings to other histological subtypes. The imaging analysis was limited to conventional grayscale and color Doppler features; quantitative elastography and standardized radiomic features were unavailable, and the unweighted composite phenotype score was exploratory and had not undergone external validation. Finally, postoperative follow-up was unavailable for the hospital-based cohort; consequently, disease-free survival, overall survival, locoregional recurrence, and distant metastasis could not be analyzed, and the present clinical findings should not be interpreted as evidence of prognostic value.

Conclusion

This study demonstrates an association between PIK3CA/TP53 mutation status and multidimensional ultrasonographic phenotypes of breast cancer. PIK3CA mutation tended to correspond to a lower burden of malignant sonographic features, whereas TP53 mutation was associated with a more aggressive ultrasound phenotype. These findings provide preliminary radiogenomic evidence that conventional ultrasonographic phenotypes may indirectly reflect molecular heterogeneity of breast cancer. Given the single-center, retrospective design, these results require prospective validation before any clinical application.

Disclosure of conflict of interest

None.

Abbreviations

ABI, Applied Biosystems; ANOVA, analysis of variance; BC, breast cancer; BLAST, Basic Local Alignment Search Tool; cDNA, complemen-

tary DNA; CD4, cluster of differentiation 4; CD8, cluster of differentiation 8; DICOM, Digital Imaging and Communications in Medicine; DNA, deoxyribonucleic acid; ER, estrogen receptor; GAPDH, glyceraldehyde-3-phosphate dehydrogenase; HER2, human epidermal growth factor receptor 2; ICC, intraclass correlation coefficient; IQR, interquartile range; LSD, least significant difference; mRNA, messenger RNA; NCBI, National Center for Biotechnology Information; PACS, Picture Archiving and Communication System; PCR, polymerase chain reaction; PI3K/AKT, phosphoinositide 3-kinase/protein kinase B; PIK3CA, phosphatidylinositol-4,5-bisphosphate 3-kinase catalytic subunit alpha; PR, progesterone receptor; qRT-PCR, quantitative reverse transcription polymerase chain reaction; RNA, ribonucleic acid; SPSS, Statistical Package for the Social Sciences; TCGA, The Cancer Genome Atlas; TCGA-BRCA, The Cancer Genome Atlas Breast Invasive Carcinoma cohort; TIMER, Tumor Immune Estimation Resource; TP53, tumor protein p53; WT, wild type.

Address correspondence to: Dr. Tao Cheng, Department of Ultrasound, Changzhou Fourth People's Hospital, No. 68 Honghe Road, Xinqiao Town, Xinbei District, Changzhou 213000, Jiangsu, China. E-mail: chengtaoczth@outlook.com

References

[1] Khan AQ, Touseeq M, Rehman S, Tahir M, Ashfaq M, Jaffar E and Abbasi SF. Advances in breast cancer diagnosis: a comprehensive review of imaging, biosensors, and emerging wearable technologies. Front Oncol 2025; 15: 1587517.

[2] Bray F, Laversanne M, Sung H, Ferlay J, Siegel RL, Soerjomataram I and Jemal A. Global cancer statistics 2022: GLOBOCAN estimates of incidence and mortality worldwide for 36 cancers in 185 countries. CA Cancer J Clin 2024; 74: 229-263.

[3] Mohd Zuhdi NF, Siddig A, Mohd Nafi SN, Md Salleh MS, Yahya MM, Wan Zain WZ, Tengku Din TADA and Wan Abdul Rahman WF. Next-generation sequencing in breast cancer: current clinical applications and future directions. Ann Med 2025; 57: 2569989.

[4] Reinhardt K, Stückrath K, Hartung C, Kaufhold S, Uleer C, Hanf V, Lantzsch T, Peschel S, John J, Pöhler M, Bauer M, Bürrig FK, Weigert E, Buchmann J, Kantelhardt EJ, Thomssen C and Vetter M. PIK3CA-mutations in breast cancer. Breast Cancer Res Treat 2022; 196: 483-493.

[5] Zwimpfer TA, Heidinger M, Coelho R, Stiegeler N, Schwab FD, Montavon C, Eller RS, Maggi N, Loesch JM, Vetter M, Lambertini M, Weber WP, Kurzeder C and Heinzelmann-Schwarz V. TP53 mutations and phosphatidylinositol 3-kinase/AKT pathway Alterations are key determinants of breast cancer outcome independent of subtype and stage. JCO Precis Oncol 2025; 9: e2400767.

[6] Bahrin NWS, Matusin SNI, Mustapa A, Huat LZ, Perera S and Hamid MRWHA. Exploring the effectiveness of molecular subtypes, biomarkers, and genetic variations as first-line treatment predictors in Asian breast cancer patients: a systematic review and meta-analysis. Syst Rev 2024; 13: 100.

[7] Malik S and Zaheer S. The impact of liquid biopsy in breast cancer: redefining the landscape of non-invasive precision oncology. J Liq Biopsy 2025; 8: 100299.

[8] Iacob R, Iacob ER, Stoicescu ER, Ghenciu DM, Cocolea DM, Constantinescu A, Ghenciu LA and Manolescu DL. Evaluating the role of breast ultrasound in early detection of breast cancer in low- and middle-income countries: a comprehensive narrative review. Bioengineering (Basel) 2024; 11: 262.

[9] Zhou J, Wu J, Zhu C and An Q. Ultrasound radiomics in the assessment of breast cancer molecular subtypes: a systematic review and meta-analysis. Med Ultrason 2025; 27: 315-322.

[10] Wang SR, Shen YT, Huang B and Xu HX. Ultrasound-based radiogenomics: status, applications, and future direction. Ultrasonography 2025; 44: 95-111.

[11] Yao J, Li X, Chai W, Li A, Chen X, Zhou W and Zhou J. Predicting PIK3CA mutation in breast cancer with machine learning based multimodal image radiomics. Eur J Med Res 2025; 30: 1161.

[12] Huang Y, Qiang Y, Jian L, Jin Z, Lang Q, Sheng C, Shichong Z and Cai C. Ultrasonic features and molecular subtype predict somatic mutations in TP53 and PIK3CA genes in breast cancer. Acad Radiol 2022; 29: e261-e270.

[13] Kostecka A, Nowikiewicz T, Olszewski P, Koczkowska M, Horbacz M, Heinzl M, Andreou M, Salazar R, Mair T, Madanecki P, Gucwa M, Davies H, Skokowski J, Buckley PG, Pęksa R, Śrutek E, Szylberg Ł, Hartman J, Jankowski M, Zegarski W, Tiemann-Boege I, Dumanski JP and Piotrowski A. High prevalence of somatic PIK3CA and TP53 pathogenic variants in the normal mammary gland tissue of sporadic breast cancer patients revealed by duplex sequencing. NPJ Breast Cancer 2022; 8: 76.

[14] Turner NC, Im SA, Saura C, Juric D, Loibl S, Kalinsky K, Schmid P, Loi S, Sunpaweravong P,

Musolino A, Li H, Zhang Q, Nowecki Z, Leung R, Thanopoulou E, Shankar N, Lei G, Stout TJ, Hutchinson KE, Schutzman JL, Song C and Jhaveri KL. Inavolisib-based therapy in PIK3CA-mutated advanced breast cancer. N Engl J Med 2024; 391: 1584-1596.

[15] Hwang SH, Baek SH, Lee MJ, Kook Y, Bae SJ, Ahn SG and Jeong J. Clinical relevance of TP53 mutation and its characteristics in breast cancer with long-term follow-up date. Cancers (Basel) 2024; 16: 3899.

[16] Jia W, Luo S, Guo H and Kong D. Development of PI3Kα inhibitors for tumor therapy. J Biomol Struct Dyn 2023; 41: 8587-8604.

[17] Marvalim C, Datta A and Lee SC. Role of p53 in breast cancer progression: an insight into p53 targeted therapy. Theranostics 2023; 13: 1421-1442.

[18] Vellichirammal NN, Tan YD, Xiao P, Eudy J, Shats O, Kelly D, Desler M, Cowan K and Guda C. The mutational landscape of a US Midwestern breast cancer cohort reveals subtype-specific cancer drivers and prognostic markers. Hum Genomics 2023; 17: 64.

[19] Filippi A and Mocanu MM. Mining TCGA database for genes with prognostic value in breast cancer. Int J Mol Sci 2023; 24: 1622.

[20] Tadesse GF, Tegaw EM and Abdisa EK. Diagnostic performance of mammography and ultrasound in breast cancer: a systematic review and meta-analysis. J Ultrasound 2023; 26: 355-367.

[21] Elayat G and Selim A. Angiogenesis in breast cancer: insights and innovations. Clin Exp Med 2024; 24: 178.

[22] Prajoko YW, Heriyanto DS, Dirja BT, Susanto S, Lau V, Gunawan AN, Halim BN and Amalina ND. High frequency of the PIK3CA H1047L mutation in Indonesian breast cancer across molecular subtypes. PLoS One 2025; 20: e0322154.

[23] Qayoom H, Haq BU, Sofi S, Jan N, Jan A and Mir MA. Targeting mutant p53: a key player in breast cancer pathogenesis and beyond. Cell Commun Signal 2024; 22: 484.

[24] Wang Y, Li Y, Song Y, Chen C, Wang Z, Li L, Liu M, Liu G, Xu Y, Zhou Y, Sun Q and Shen S. Comparison of ultrasound and mammography for early diagnosis of breast cancer among Chinese women with suspected breast lesions: a prospective trial. Thorac Cancer 2022; 13: 3145-3151.

[25] Xia S, Hua Q, Song Y, Yuan C, Zheng Y, Tao R, Xu J, Cai E, Zhang Y, Wu F, Guo W, Tian Y, Dong Y and Zhou J. Super-resolution ultrasound imaging of intranodal lymphatic sinuses for predicting sentinel lymph node metastasis in breast cancer: a preliminary study. Eur Radiol 2025; 35: 6079-6088.

Supplementary Table 1. Molecular subtype-adjusted associations between PIK3CA/TP53 mutation status and ultrasonographic phenotype burden

Ultrasonographic feature	PIK3CA Holm-adjusted P	TP53 Holm-adjusted P	
Irregular shape	<0.001	<0.001	
Spiculated margin	<0.001	<0.001	
Heterogeneous echogenicity	0.157	0.002	
Microcalcification	0.001	0.004	
Posterior acoustic attenuation	0.018	0.169	
Aspect ratio ≥1	0.493	<0.001	
Adler blood-flow grade II–III	<0.001	0.032	
Combined mutation pattern	Adjusted OR for a higher phenotype-score category	95% CI	Holm-adjusted P
Double wild type	Reference	-	-
PIK3CA-only mutant	0.17	0.09-0.33	<0.001
TP53-only mutant	13.23	6.09-28.72	<0.001
Double mutant	3.48	1.21-9.99	0.02

The ordinal logistic model was adjusted for molecular subtype. Because the double-mutant subgroup contained only 12 patients, its estimate should be interpreted as exploratory.

Supplementary Table 2. Interobserver and intraobserver agreement for ultrasonographic features

Ultrasonographic feature	Statistic	Interobserver agreement, %	Interobserver κ (95% CI)	Intraobserver agreement, %	Intraobserver κ (95% CI)
Lesion-size category	Linear weighted κ	80.5	0.719 (0.520-0.876)	92.7	0.894 (0.756-1.000)
Lesion shape	Cohen's κ	90.2	0.765 (0.509-0.947)	97.6	0.942 (0.796-1.000)
Lesion margin	Cohen's κ	90.2	0.800 (0.584-0.951)	92.7	0.848 (0.656-1.000)
Internal echogenicity	Cohen's κ	80.5	0.612 (0.368-0.835)	92.7	0.840 (0.648-1.000)
Microcalcification	Cohen's κ	80.5	0.608 (0.344-0.848)	92.7	0.854 (0.691-1.000)
Posterior acoustic feature	Cohen's κ	90.2	0.796 (0.581-0.951)	92.7	0.845 (0.647-1.000)
Aspect-ratio category	Cohen's κ	95.1	0.901 (0.750-1.000)	87.8	0.752 (0.530-0.945)
Adler blood-flow grade	Cohen's κ	87.8	0.757 (0.520-0.949)	90.2	0.805 (0.604-0.951)

Values are percentage agreement or kappa coefficients with 95% confidence intervals. Interobserver agreement was calculated between the first independent assessments of Readers 1 and 2, whereas intraobserver agreement was calculated between the two assessments of Reader 1 performed at least 2 weeks apart. Linear weighted kappa was used for the three-level lesion-size category, and unweighted Cohen's kappa was used for the remaining binary features. Confidence intervals were obtained using 2,000 nonparametric bootstrap resamples. ICC was not applicable because no continuous ultrasonographic variables were included.